RESEARCH ARTICLE

Dynamics of simulated Atlantic upwelling annual cycle in CMIP5 models

Li-Chiao Wang[1] [ID], **Fei-Fei Jin[2]** [ID], **and Chau-Ron Wu[1]** [ID]

[1]Department of Earth Sciences, National Taiwan Normal University, Taipei, Taiwan, [2]Department of Atmospheric Sciences, University of Hawaii at Manoa, Honolulu, Hawaii

Abstract As one of the prominent climatic component of tropical climate system, the annual cycle of the equatorial Atlantic cold tongue region has been a subject of significant research. In this work, we examine the fidelity of the key part of the annual cycles, namely, the upwelling annual cycles, from the simulations of the Coupled Model Intercomparison Project Phase 5 (CMIP5). Utilizing the simple framework we have recently developed based on the Zebiak-Cane (ZC) ocean model, we first tested the validity of the simple framework of upwelling as a combination of the local wind-driven Ekman upwelling and nonlocal wind-driven wave upwelling. It is demonstrated that the theoretically reconstructed upwelling annual cycles to large extent are in good agreement with the simulations in these coupled climatic models. Comparing with observations, we show that the semiannual component of the upwelling is systematically too strong. This significant bias is attributable to the dynamic amplification to the wind-driven wave upwelling originated from a less significant bias in the semiannual harmonic component in the central equatorial wind field. The latter is dynamically amplified in the wind-driven wave upwelling owing to its relatively fast time scale. Thus, the realistic simulations of equatorial annual cycles may sensitively depend on good simulations of the semiannual harmonic components in equatorial wind fields.

1. Introduction

Equatorial upwelling plays a key role in the cold tongue development and therefore influences the entire tropical climatic system. Upwelling peaks in early boreal summer, and the cold tongue sea surface temperature (SST) attains a minimum immediately thereafter. This indicates that dynamic cooling is important in phasing of the equatorial cold tongue SST annual cycle [*Clement et al.*, 1997; *An et al.*, 2012]. Variations in equatorial upwelling are closely associated with nutrient concentrations and primary productivities [*Dandonneau et al.*, 2004].

Great progress has been made in analyzing variations in equatorial upwelling. It is generally accepted that such upwelling is largely attributable to Ekman pumping driven by local winds [*Weingartner and Weisberg*, 1991; *Richter and Xie*, 2008; *Hagos and Cook*, 2009]. However, the basic dynamics of the equatorial Atlantic upwelling annual cycle remain poorly understood despite the essential role played by the annual cycle in the equatorial Atlantic climate.

A recent study developed a simple framework of the equatorial Atlantic upwelling annual cycle based on the Zebiak-Cane (ZC) ocean model [*Zebiak and Cane*, 1987, hereinafter ZC87], as a combination of local wind-driven Ekman upwelling and nonlocal wind-driven wave upwelling [*Wang et al.*, 2017]. They also demonstrated in observations that Ekman upwelling predominates in the western equatorial Atlantic, whereas wave upwelling is key in the eastern equatorial Atlantic. In the present work, we explored the validity of the simple upwelling framework in the Coupled Model Intercomparison Project Phase 5 (CMIP5) simulations. It is essential to evaluate the ability of the model to simulate the equatorial upwelling annual cycle, since this is closely related to the ability of the model to predict the cold tongue SST development. We therefore also discussed whether CMIP5 could simulate the equatorial Atlantic upwelling annual cycle and clarified what was required to allow CMIP5 models to afford realistic simulations.

The remainder of this paper is organized as follows. In section 2, we describe the data set used. The theoretically reconstructed equatorial Atlantic upwelling annual cycles of CMIP5 simulations are analyzed in section 3. Section 4 explores the dynamic reasons for the introduction of systematic bias into model simulations

Table 1. List of the CMIP5 Models Analyzed in the Study

Model Name	Modeling Center
ACCESS1-0	The Centre for Australian Weather and Climate Research, Australia
ACCESS1-3	
bcc-csm1-1	Beijing Climate Center, China Meteorological Administration, China
bcc-csm1-1-m	
CanESM2	Canadian Centre for Climate Modelling and Analysis, Canada
CCSM4	National Center for Atmospheric Research, USA
CESM1-BGC	
CESM1-CAM5	
CESM1-FASTCHEM	
CESM1-WACCM	
CMCC-CESM	Centro Euro-Mediterraneo per I Cambiamenti Climatici, Italy
CMCC-CM	
CMCC-CMS	
FGOALS-g2	LASG, Institute of Atmospheric Physics, Chinese Academy of Sciences, China
GFDL-ESM2M	NOAA Geophysical Fluid Dynamics Laboratory, USA
GISS-E2-R	NASA Goddard Institute for Space Studies, USA
GISS-E2-R-CC	
HadGEM2-CC	Met Office Hadley Centre, UK
HadGEM2-ES	
IPSL-CM5A-LR	Institut Pierre-Simon Laplace, France
IPSL-CM5A-MR	
IPSL-CM5B-LR	
MRI-CGCM3	Meteorological Research Institute, Japan
NorESM1-M	Norwegian Climate Centre, Norway
NorESM1-ME	

and shows how the models can be made realistic. Section 5 discusses the role of recharge/discharge in the upwelling annual cycle of CMIP5 models. A conclusion (section 6) follows.

2. Model and Data

We analyzed a series of historical experiment simulations from 25 CMIP5 models during the period roughly of 1950–2005. See *Taylor et al.* [2012] for the relevant model descriptions and experiment designs. We mainly focused on the performance of CMIP5 multimodel ensemble (MME). The results of each individual and mean averaged by 25 models are also discussed. The data from all model output were interpolated onto a $1° \times 1°$ grid. Detailed information about the analyzed models is given in Table 1.

The observational data including vertical velocity, SST, wind stresses, and 20°C isotherm depth, which represents the thermocline depth, were obtained from the European Centre for Medium-Range Weather Forecasts (ECMWF) operational ocean analysis/reanalysis system (ORA-S3) [*Balmaseda et al.*, 2008, for the period 1959–2009]. ORA-S3 is based on the Hamburg Ocean Primitive-Equation (HOPE) model [*Wolff et al.*, 1997] and forced by daily fluxes of momentum, heat, and freshwater. The horizontal resolution was $1° \times 1°$. There are 29 levels in the vertical direction, with a typical vertical thickness of 10 m in the upper ocean [*Balmaseda et al.*, 2008]. The fine equatorial resolution of ORA-S3 is important in analyzing the ocean-atmosphere dynamics in tropical Pacific [*Zhai and Hu*, 2013; *Jin et al.*, 2014]. It is also frequently used to resolve the prominent Atlantic variability in northern [*Balmaseda et al.*, 2007; *Muñoz et al.*, 2011] and equatorial [*Nnamchi et al.*, 2015, 2016] area, and thus will be also utilized for this study. The annual cycles were defined in this work as the anomalies with respect to the climate annual mean of the entire data period.

3. Equatorial Upwelling Annual Cycles in CMIP5 Simulations

3.1. Simulated Upwelling Annual Cycles

We begin with a simple comparison between the observed and CMIP5 simulations of the upwelling annual cycles depicted by the longitude-time evolution patterns (Figure 1). The model simulations, although roughly capture the observed equatorial annual upwelling evolution patterns, clearly display some significant biases. In most models (about 20 out of 25 models), the simulated equatorial Atlantic annual cycles were dominated by a strong annual harmonic component in the west and an evident semiannual harmonic component in the east (four rows starting from row (b)). The others (row (c)) either produced a relatively inaccurate phasing in the second half of the year or simulated relatively weak upwellings (including GISS-E2-R and GISS-E2-R-CC). This is attributable to the weaker equatorial wind stress forcing, resulting in a flanker thermocline, weaker upwelling, and SST variability. Similar dynamics has been discussed in previous studies [*Grodsky et al.*, 2012; *Li and Xie*, 2012; *Muñoz et al.*, 2012; *Voldoire et al.*, 2014]. Our result also agrees with *Richter et al.* [2014] that they found there is a near-zero correlation between the equatorial surface winds and the cold tongue meridional SST gradient in boreal spring in two GISS models (see their Figure 9). The weaker wind field and deeper mean thermocline located in cold tongue region [*Richter et al.*, 2014] make their Bjekness process not as sharp as other models in equatorial Atlantic.
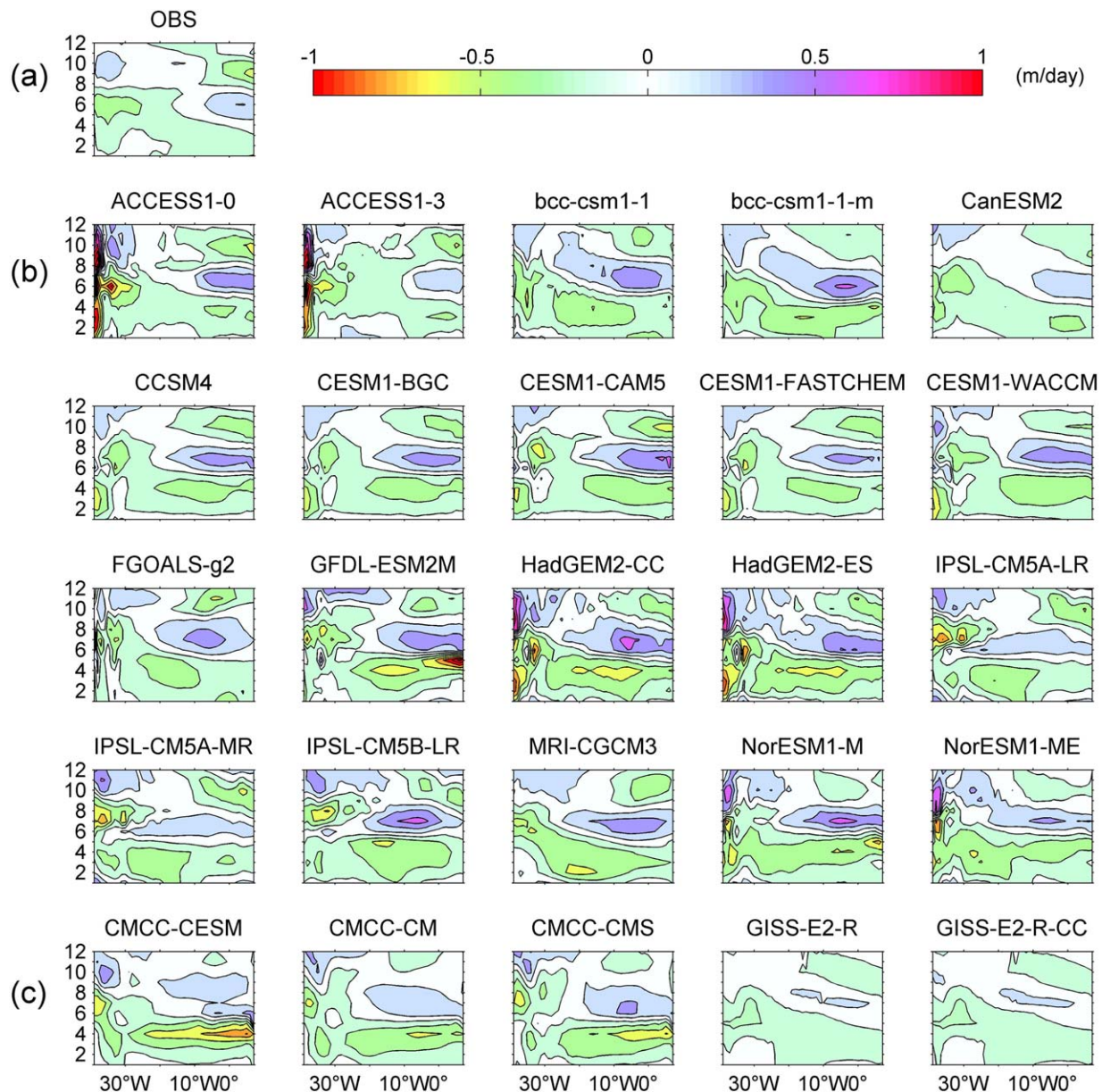
Figure 1. Time-longitude diagrams of the equatorial Atlantic upwelling annual cycles (averaged in the band 3°N–3°S) from (a) observation and originally simulated by 25 CMIP5 models, including 20 models that have more realistic Atlantic upwelling annual cycle simulations (four rows starting from row (b)) and the others (row (c)).

3.2. Theoretical Upwelling Annual Cycles

The framework proposed by *Wang et al*. [2017] for the upwelling annual cycle in the equatorial Atlantic is a combination of local wind-driven Ekman upwelling and nonlocal wind-driven wave upwelling based on the ZC87 model:

$$W = W_e \cdot [1 - R(x)] + W_h \cdot R(x) \tag{1}$$

$$R(x) = H_1 / H(x) = 50 / H(x) = 1 \quad \text{if } H(x) < 50 \tag{2}$$

This upwelling is represented by a linear combination of the Ekman and wave upwelling, denoted W_e and W_h respectively. The wave upwelling can be expressed as $-\partial h/\partial t$ (h denotes the thermocline depth), namely, the negative thermocline tendency. Here H and H_1 refer, respectively, to the mean climatic thermocline depth and the constant mixed layer depth. This formulation of upwelling is essentially the same as that of ZC87, except that here, zonal variations in the climatic mean of the thermocline depth are taken into

consideration so that the weighting function $R(x)$ now also depends on longitude (see supporting information A for more details). To obtain the theoretically reconstructed equatorial vertical velocity as formulated in equation (1), we need to use (1) the surface wind stress to calculate the Ekman upwelling W_e following the formulation of ZC87, (2) the thermocline depth to calculate W_h, and (3) the climatic mean depth of the thermocline $H(x)$ to calculate $R(x)$. It is important to keep in mind that the contributions of the Ekman and wave upwellings to the total vertical velocity are further weighted by functions $1-R(x)$ and $R(x)$, respectively, which weigh heavily on Ekman upwelling in the west and wave upwelling in the east.

We applied this simple framework to both observation and the CMIP5 simulations of the Atlantic upwelling annual cycle (Figure 2). The observed equatorial Atlantic upwelling annual cycle was dominated by a strong annual harmonic component in the west and a significant semiannual harmonic component in the east (Figure 2a). Both features were captured by the theoretically reconstructed vertical velocity (Figure 2b). The time-longitude evolution of the pattern correlation (simply termed the pattern correlation hereafter) between the observed and theoretically reconstructed vertical velocity was 0.82, indicating that the simple
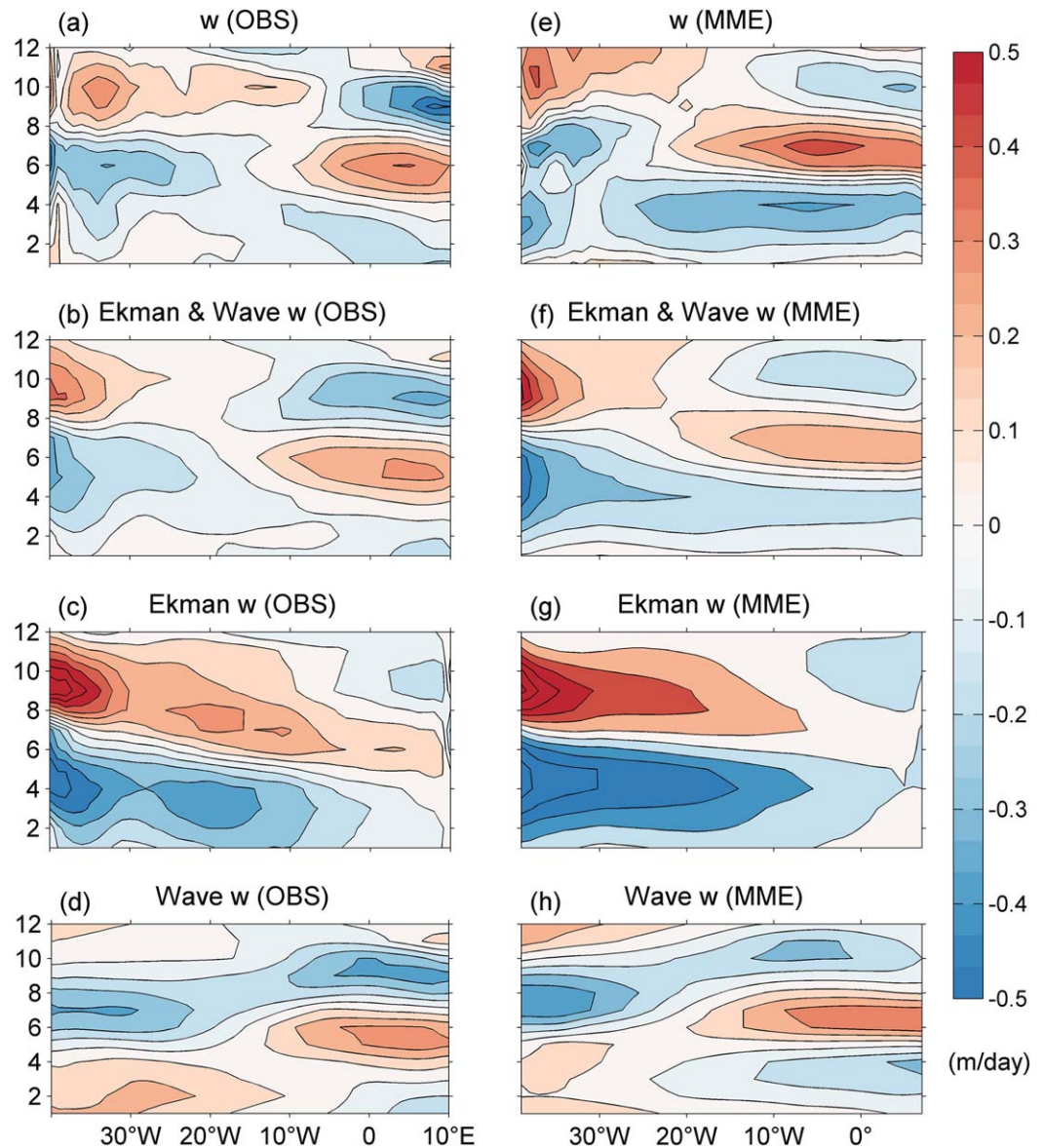

Figure 2. Time-longitude diagrams of the annual cycles of the (a, e) original, (b, and f) theoretical, (c, and g) Ekman, and (d, and h) wave upwellings in the equatorial Atlantic averaged over 3°N–3°S and derived via observation and the CMIP5 MME, respectively (unit: m/d).

framework of equation (1) is reasonably successful. To measure the dominance of Ekman and wave upwelling in each side of the basin, we define the relative contribution of the two parts of the upwelling in the following manner:

$$r = \frac{|We|^2}{|We|^2 + |Ww|^2} \tag{3}$$

where $|We|$ and $|Ww|$ are amplitudes of Ekman and wave component averaged over the annual cycle in the western and eastern basins. Then automatically r is for the Ekman contribution and $1-r$ is for the wave contribution. In observation, r is about 63% in the western basin, indicating the western Atlantic is predominated by the Ekman upwelling; in the east, $1-r$ is 89%, indicating the eastern Atlantic is predominated by the wave upwelling. The Ekman upwelling (Figure 2c) is dominated in the western Atlantic by an annual harmonic component with a phase similar to that of the observed upwelling. The Ekman upwelling is much weaker in the eastern Atlantic. The pattern correlation between the observed vertical velocity (Figure 2a) and the derived Ekman upwelling was about 0.53, clearly showing that Ekman effect alone was inadequate to characterize the equatorial upwelling annual cycle in the Atlantic. In contrast, wave upwelling (Figure 2d) yielded a strong semiannual signal in the eastern Atlantic, with a phase similar to that of the observed upwelling. Nevertheless, the pattern correlation between the observed vertical velocity and the wave upwelling was only about 0.56, again indicating that wave effect alone inadequately characterized the equatorial upwelling annual cycle in the Atlantic.

The MME exhibited a pattern consistent with observation (Figures 2e–2h), but a slightly overestimation of amplitudes. The amplitude of the original upwelling in MME is about 17% stronger than in observation, and the theoretically reconstructed upwelling in MME is about 12% stronger than in observation. In MME, r is about 73% in the western basin, indicating the western Atlantic is also predominated by the Ekman upwelling; in the east, $1-r$ is 83%, indicating the eastern Atlantic is predominated by the wave upwelling as well. However, a systematic bias was apparent in the semiannual harmonic components of the model-simulated, theoretically reconstructed and wave upwelling (Figures 2e, 2f, and 2h), compared to observed upwelling annual cycles. The amplified semiannual harmonic component of MME in the eastern Atlantic was well characterized by the simple framework proposed by *Wang et al.* [2017]; the pattern correlation between the original and theoretically reconstructed values was 0.84. Thus, the simple framework successfully characterized the equatorial upwelling annual cycle pattern in model simulations. Moreover, wave upwelling explained the amplified semiannual harmonic component (Figure 2h) since the derived Ekman upwelling dominated in the western Atlantic (Figure 2g). The pattern correlation between the original and the Ekman/wave upwelling was 0.53/0.61. It is worth noticing that the spatial distribution of the semiannual harmonic component in the MME pattern (shown in original, theoretical and wave upwelling) shifted westward compared to observational pattern and reached 25°W.

In terms of individual simulations, Figure 3 lists the pattern correlations between the originally simulated and theoretically reconstructed equatorial upwellings of 25 CMIP5 models. Evidently, most models adequately reproduced the upwelling annual cycle in the equatorial Atlantic; the pattern correlations were >0.7. Some of the model simulations showed relatively diverse patterns. The Ekman and wave components computed from the ACCESS-1-3 outputs did not capture the equatorial Atlantic pattern very well (both correlations were ~0.4). Therefore, the linear combination also exhibited a relatively low correlation (0.58) with the originally simulated upwelling (not shown). On the other hand, the original upwellings from the IPSL-CM5A-LR, IPSL-CM5A-MR, and IPSL-CM5B-LR simulations were all dominated by the wave component of the entire Atlantic basin; the correlations were ~0.7. In contrast, the correlation with the theoretically reconstructed upwelling was actually lower (~0.5) after the Ekman component was included. This is resulted from a positive bias in the meridional wind shear divergence, resulting in the out of phase of the Ekman component and the original upwelling simulated by IPSL series models (figure not shown). The mean correlation between the model-simulated and theoretically reconstructed upwellings yielded by all CMIP5 models was 0.74. Moreover, the MME theoretical upwelling also yielded a good correlation (0.84), even higher than that in observation (0.82). These results show that, in observation and model simulations, the weighted combination framework captures contributions from both Ekman and wave upwelling and can be used to successfully characterize the equatorial upwelling annual cycle pattern.
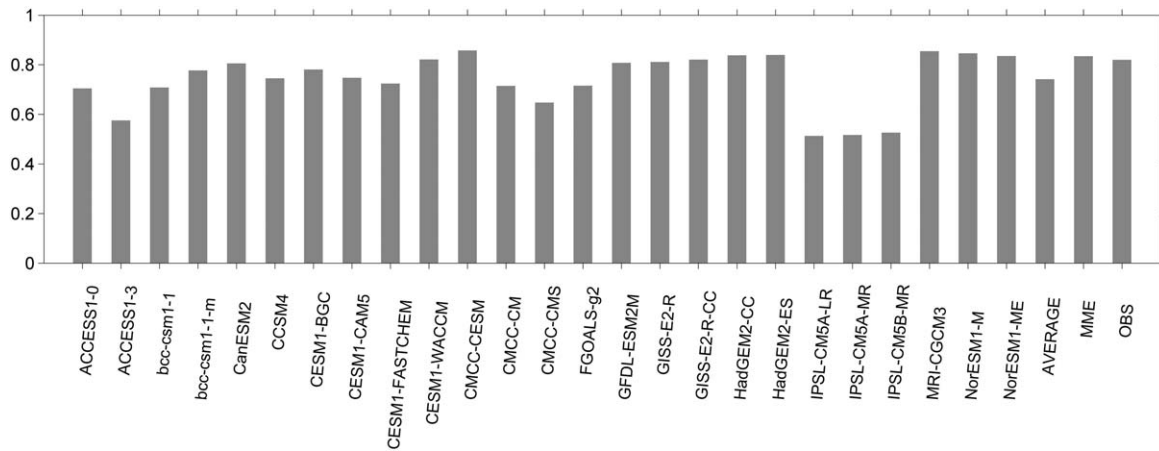
Figure 3. A bar chart showing correlations between the original and theoretical values of the equatorial upwelling annual cycles from 25 CMIP5 models and the observation.

Figure 4 contrasts the different contributions made by Ekman upwelling in the west and wave upwelling in the east in terms of both observation and MME. In the west, both Ekman and wave effects are important. In observation, the Ekman upwelling attains a maximum 1 month before the observed upwelling peaks, and is a principal contributor to the development of peak upwelling. Wave upwelling appears to contribute negatively (thus canceling some of the Ekman upwelling) and makes the theoretically reconstructed upwelling consistent with the observation (Figure 4a). In the eastern equatorial Atlantic, wave upwelling dominates the observed upwelling annual cycle; Ekman upwelling contributes very little (Figure 4b).
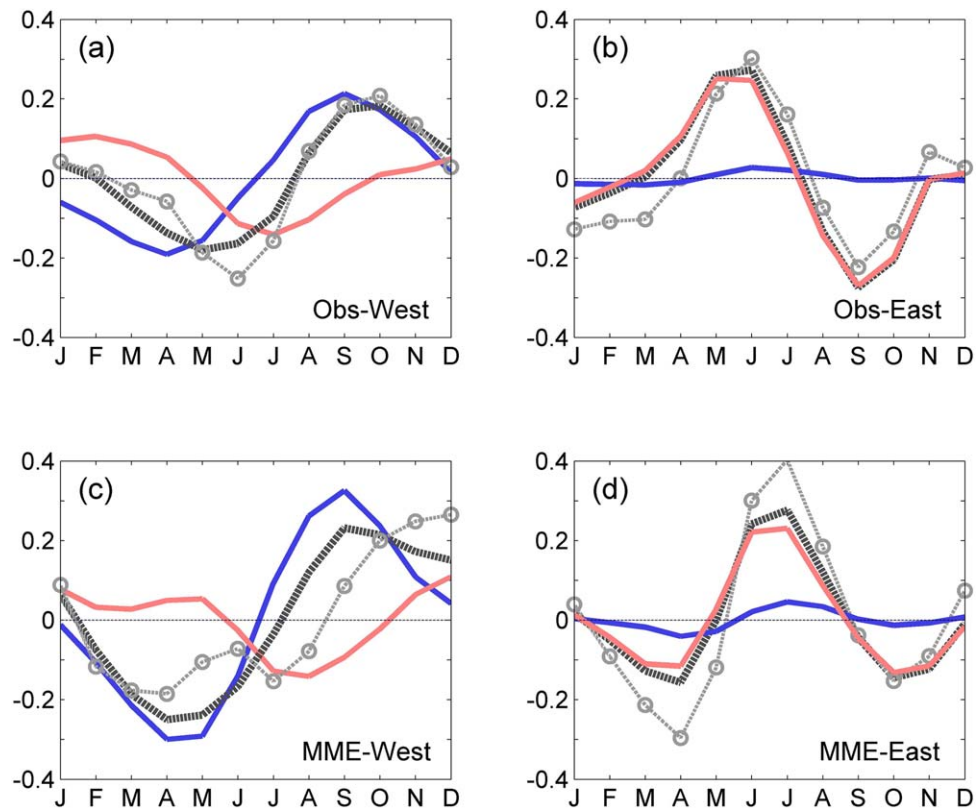

Figure 4. The equatorial Atlantic annual cycles of original (gray circle), theoretical (dashed black), Ekman (blue), and wave (pink) upwellings over western (3°N–3°S, 30°W–10°W) and eastern (3°N–3°S, 10°W–10°E) regions, (a, and b) as observed and (c, and d) as derived using CMIP5 MME averages, respectively (unit: m/d).

In the western Atlantic, MME yielded data similar to observations, although the Ekman upwelling was of relatively large amplitude (Figure 4c). This was mostly attributable to the stronger equatorial wind field used in simulation. The amplitude of the zonal/meridional wind stress from MME is about 25%/28% stronger than observation near the western boundary (not shown). The bias in the equatorial wind fields is likely to intensify the Ekman upwelling and induce perturbations in the original upwelling in the western Atlantic. In the east, wave upwelling dominated the originally simulated upwelling annual cycle, in accord with observation. However, wave upwelling exhibits a 1–2 months phase shift compared to the observation. This explains the large semiannual harmonic component of the upwelling annual cycle in the eastern equatorial Atlantic apparent in CMIP5 simulations (Figure 4d). We will discuss this topic further in section 5.

4. Dynamics of Wave Upwelling in CMIP5 Models

4.1. Shallow-Water Modeling

To further examine the influence of equatorial upwelling dynamics on wave upwelling, a shallow-water model (SWM) [*McGregor et al.*, 2007] forced by observed wind stresses (from ORA-S3) was used to simulate wave upwelling. To render the model applicable to the tropical Atlantic basin, we reduced the gravity wave speed by a factor of 0.6. This meant that the thermocline depth simulated by the SWM was comparable to observations. The SWM successfully captured the annual evolution of the equatorial thermocline (Figures 5a–5f, shading). The pattern correlation between the CMIP5 MME and the total thermocline depth modeled by the SWM was 0.9. We further decomposed the total thermocline depth into annual and semiannual components, and continued to find good agreement between CMIP5 MME and SWM. The pattern correlations of annual and semiannual components were 0.9 and 0.84, respectively.

The important point here is the remarkable agreement between the originally simulated and the SWM modeled wave upwellings (Figures 5a–5f, contours). The pattern correlation between the CMIP5 MME and the total thermocline depth tendency modeled by the SWM was 0.85, and those for the annual and semiannual components 0.9 and 0.8, respectively. These results indicate that the strong semiannual harmonic bias evident in the wave upwelling originally simulated by the MME is, to a large extent, associated with the input wind field.

4.2. The Semiannual/Annual Harmonic Component Amplitude Ratio (SAR)

In the CMIP5 MME pattern, wave upwelling exhibited a significantly amplified, semiannual harmonic signal (Figure 4d), which contributed to the equatorial upwelling annual cycle in model simulations (Figures 2e and 4d). To better quantify this contribution, we calculated the standard deviation ratio of semiannual to annual harmonic component amplitudes, defined as

$$ratio = \frac{\sigma_S}{\sigma_A} \tag{4}$$

where A and S denote the annual and semiannual harmonic components, respectively. The semiannual/annual harmonic component amplitude ratio (SAR) was defined as the standard deviation (σ) of the semiannual harmonic component amplitude divided by the standard deviation of the annual harmonic component amplitude. We considered three different regions: the western, central, and eastern equatorial Atlantic (3°N–3°S, 40°W–20°W; 3°N–3°S, 30°W–0°E; and 3°N–3°S, 10°W–10°E, respectively). Figure 6a is the scatterplot showing the relationship between the SAR of the equatorial central basin wind stress and the SAR of the eastern basin thermocline depth, which was 0.83. Although the various models performed differently, such a high correlation indicates a close connection between the SAR of the central basin winds and the SAR of the eastern thermocline depth.

Furthermore, the scatterplot of the SARs between eastern thermocline depth and its tendency confirmed that the SAR of the eastern thermocline depth tendency was almost twice as great as that of the eastern thermocline depth (Figure 6b). This makes wave upwelling from the semiannual component of thermocline fluctuation twice as effective as the annual component (a detailed explanation is given in supporting information B).

Figure 6c shows the SARs for the central basin wind stress, the eastern thermocline depth, and the eastern thermocline depth tendency in CMIP5 models. From (3), the following relationships are evident:
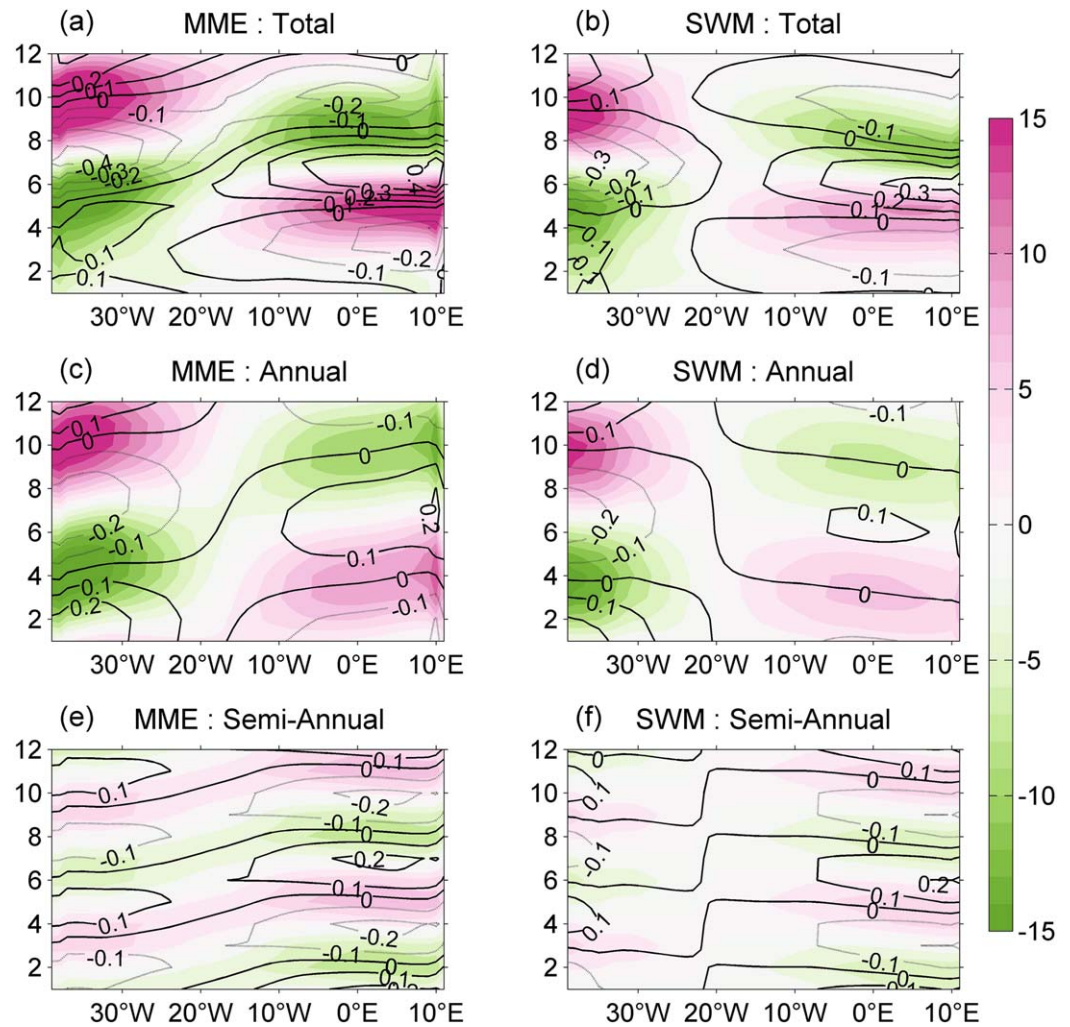
$$SAR_{h_e} = 1.7 \times SAR_\tau \tag{5}$$

Figure 5. Time-longitude diagrams of the total, annual, and semiannual components in the equatorial Atlantic annual cycles (averaged over the region 3°N–3°S) of the thermocline depth (shadings, units: m) and wave upwelling estimated via thermocline tendencies (contours; unit: m/d). (a, c, and e) CMIP5 MME average; (b, d, and f) SWM simulations.

$$SAR_{W_h} = 1.9 \times SAR_{h_e} \tag{6}$$

and we therefore obtain

$$SAR_{W_h} = 3.23 \times SAR_\tau \tag{7}$$

Equations (4–6) imply that if the SAR of the central wind field is >0.31 (red line), it is very possible that the SAR of wave upwelling will be >1 (gray line), implying that the semiannual signal overtakes the annual signal. Almost all models fall into this category, whereas the CMCC-CESM and the observed SAR of wave upwelling are <1. This significant bias is caused by less significant bias in the semiannual harmonic component of the central equatorial wind field. It appeals that the relationship between wind field and thermocline (Figure 6a) is not as robust as the relationship between thermocline and wave upwelling (Figure 6b). The dynamic amplification from wind to thermocline is weak in these two cases. Dynamic amplification renders upwelling very sensitive to errors in the semiannual wind forcing.

5. Meridional Recharge/Discharge and Zonal Mass Redistribution in Wave Upwelling

Following *Wang et al.* [2017], we further evaluated and contrasted the observed and the MME-modeled dynamic performance of the eastern Atlantic wave upwelling through the El Niño Southern Oscillation
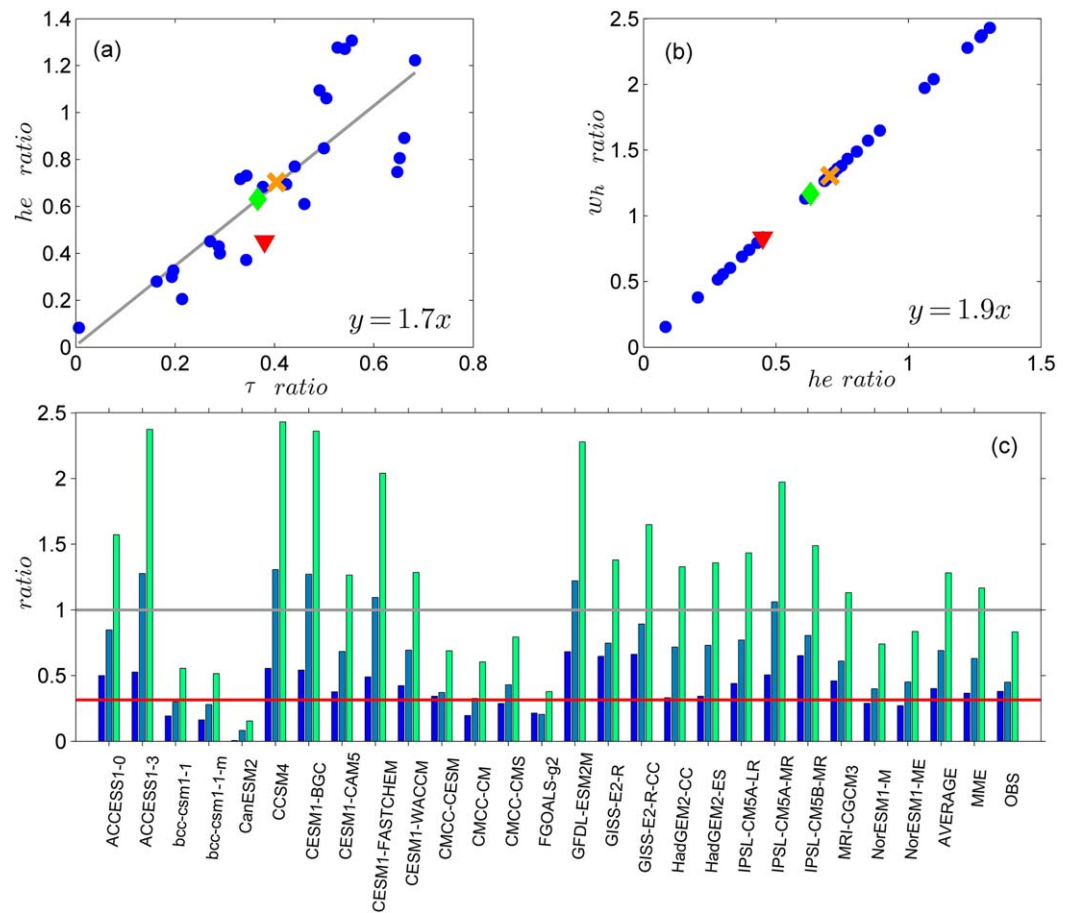
Figure 6. The semiannual/annual harmonic ratios (SARs) between (a) the central basin wind stress and eastern thermocline depth; (b) the eastern thermocline depth and the eastern wave upwelling. Green diamond, orange cross, and red triangle denote the SAR of MME, mean-averaged SAR, and observation, respectively. (c) The SARs of the central basin wind stress (blue), the eastern thermocline depth (aquamarine), and eastern wave upwelling (green) in 25 CMIP5 models and the observation. Red line (0.31) and gray line (1) highlight the thresholds when the SAR of the central wind field meets the red line, it is very possible that the SAR of wave upwelling will meet the gray line, implying the semiannual signal overtakes the annual signal in wave upwelling.

(ENSO) recharge oscillator developed by *Jin* [1997]. We examined wave upwelling in the eastern Atlantic employing the approach first developed by *Jin* [1996] and thereafter fully developed by *Jin* [1997]. This simple formulation allows us to understand the heat content dynamics associated with the ENSO recharge oscillator. *Jin* [1997] explained that the evolution of the equatorial thermocline could be understood in terms of the fast buildup of zonal contrast of thermocline depth through mass redistribution in zonal direction by the equatorial Kelvin and Rossby waves and slow meridional recharge/discharge to control the equatorial zonal mean of the thermocline depth. This allows us to express the eastern thermocline depth (tendency) in terms of the central basin wind stress (tendency) and the zonal mean thermocline (tendency); details are provided in supporting information C. As mentioned in section 4.2, we defined western, central, and eastern equatorial Atlantic regions as, respectively, 3°N–3°S, 40°W–20°W; 3°N–3°S, 30°W–0°E; and 3°N–3°S, 10°W–10°E, both observationally and for CMIP5 MME.

The zonal contrast of the thermocline is in quasi-equilibrium with the central basin wind stress, indicating that the contrast is achieved by relatively rapid wave adjustment. This was confirmed both by the MME (Figure 7a, orange) and observationally (Figure 7a, green). Furthermore, the eastern basin thermocline (tendency) can be expressed as a combination of the zonal mean thermocline depth (tendency) and the central basin wind stress (tendency) (Figure 7b), as confirmed both by the MME (diamonds) and observationally (crosses). The eastern wave upwelling can be understood in terms of the meridional discharge/recharge associated with shoaling and deepening of the zonal mean thermocline together with rapid zonal mass redistribution caused by wind-forced thermocline contrasts. The correlations of the upwelling in the eastern
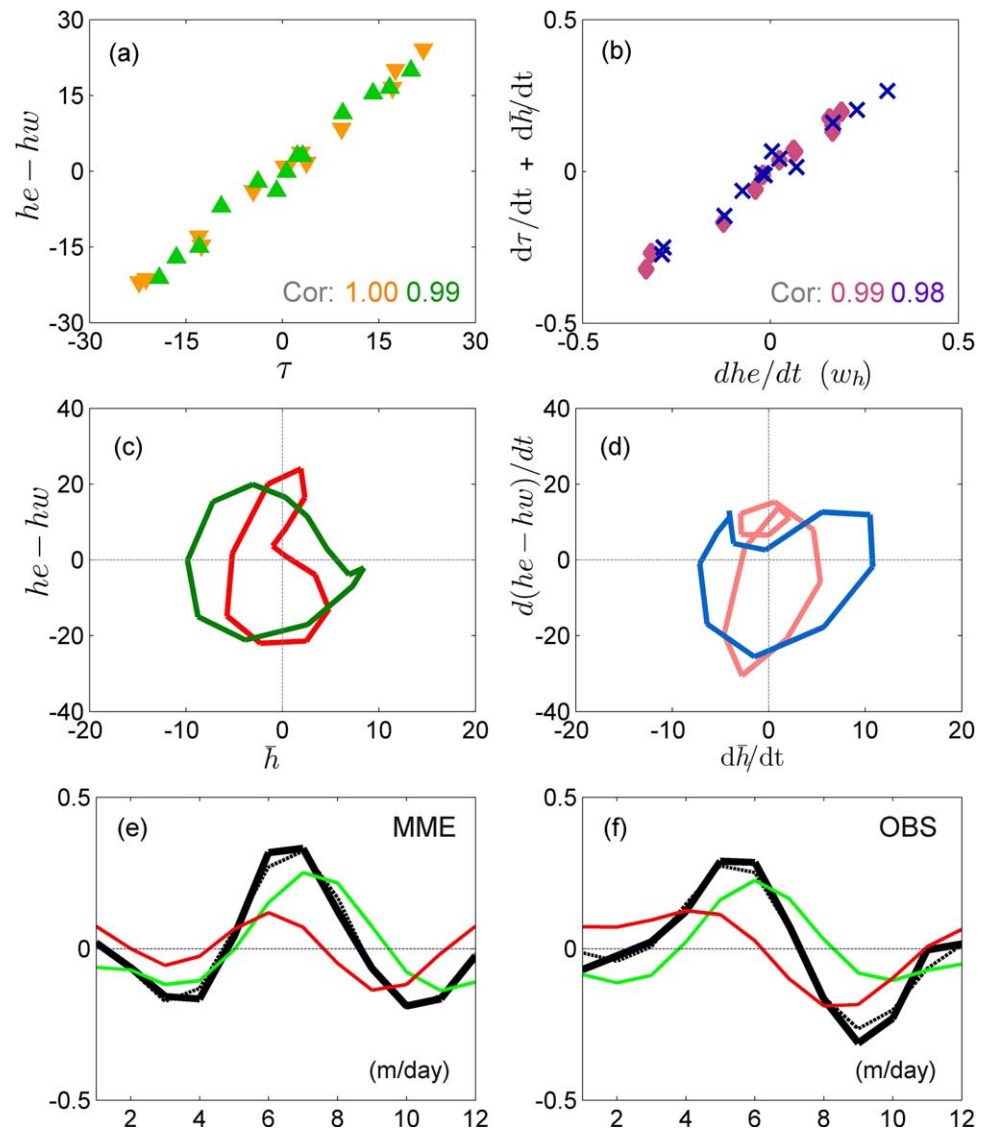
Figure 7. The relationships between (a) the central basin wind stress and zonal thermocline contrasts from MME (orange) and observation (green); (b) the wave upwelling calculated via eastern basin thermocline tendency and via application of zonal mean thermocline tendency together with the central basin wind stress tendency from MME (diamonds) and observation (crosses); (c) the zonal contrasts and zonal means of the equatorial thermocline from MME (red) and observation (green); and (d) the tendencies of zonal contrasts and zonal means of the equatorial thermocline from MME (pink) and observation (blue). (e, f) Further compares/contrasts the real (thick black lines) and estimated (black dashed lines) wave upwellings, and the two upwelling components attributable to the zonal mean thermocline tendency (red) and the central basin wind stress tendency (green). Both the MME (Figure 7e) and observed (Figure 7f) findings are shown. The measurement unit is m/d.

basin derived using this simple balance equation with the MME and observed eastern wave upwelling were 0.99 and 0.98, respectively.

Observationally, the annual cycles in zonal contrast and zonal mean of the equatorial thermocline are in 90° phase quadrature in the ENSO recharge oscillator (Figure 7c, green). The same held true for the tendencies (Figure 7d, blue). Thus, the essential process of ocean heat recharge/discharge for the ENSO recharge oscillator apparently engages, playing an important role in the observed eastern Atlantic upwelling. In the MME, the strengthened semiannual signal in the eastern equatorial thermocline (Figure 7c, red) and its tendency (Figure 7d, peach) implies that the recharge oscillator still works in the CMIP5 MME, but it is much weaker than under observational circumstances.

Figures 7e and 7f show wave upwelling (thick black lines); the two components associated with upwelling caused by the zonal thermocline contrast tendency (expressed in terms of the central basin wind stress

tendency; green line) and the zonal mean thermocline depth tendency (red line). Both processes contribute substantially to wave upwelling with the recharge/discharge process playing a crucial role in the wave upwelling and, consequently, in the entire eastern Atlantic upwelling annual cycle. In the MME (Figure 7e), both the zonal contrast and the zonal mean of the equatorial thermocline have phase shifts, illustrating an apparent semiannual harmonic signal compared to observation (Figure 7f), which contributes to the semi-annual bias in the wave upwelling annual cycle.

6. Conclusions

The Atlantic equatorial upwelling and its annual cycle are key dynamic features of tropical climatic systems and marine ecosystems. *Wang et al.* [2017] proposed a simple framework based on the ZC87 model to describe essential controls on the Atlantic equatorial upwelling annual cycle: local wind-driven Ekman upwelling and nonlocal wind-driven wave upwelling. In this work, we confirmed the validity of this simple framework in both observation and CMIP5 simulations.

The theoretical upwelling annual cycles were generally in good agreement with both observations and model simulations in coupled climatic models. However, the semiannual components of the upwelling in model simulations are systematically too strong. We further demonstrated that such significant bias is attributable to less significant bias in the semiannual harmonic component of the central equatorial wind field. Thus, realistic simulation of the equatorial upwelling annual cycle is very sensitive to careful simulation of the semiannual harmonic component of the equatorial wind field.

Observed wave upwelling plays a key role in the Atlantic SST annual cycle. In the CMIP5 models, the recharge oscillator in the wave upwelling is still at work, but its effect is weakened by the amplified semian-nual harmonic component in the wave upwelling due to the dynamic amplification originated from semian-nual harmonic component in the central wind field.

References

An, S. I., J. W. Kim, S. H. Im, B. M. Kim, and J. H. Park (2012), Recent and future sea surface temperature trends in tropical Pacific warm pool and cold tongue regions, *Clim. Dyn.*, *39*(6), 1373–1383, doi:10.1007/s00382-011-1129-7.

Balmaseda, M. A., G. C. Smith, K. Haines, D. Anderson, T. N. Palmer, and A. Vidard (2007), Historical reconstruction of the Atlantic Meridional Overturning Circulation from the ECMWF operational ocean reanalysis, *Geophys. Res. Lett.*, *34*, L23615, doi:10.1029/2007GL031645.

Balmaseda, M. A., A. Vidard, and D. L. T. Anderson (2008), The ECMWF ocean analysis system: ORA-S3, *Mon. Weather Rev.*, *136*, 3018–3034, doi:10.1175/2008MWR2433.1.

Clement, A. C., R. Seager, M. Cane, and S. E. Zebiak (1997), An ocean dynamical thermostat, *Oceanogr. Lit. Rev.*, *6*(44), 556, doi:10.1175/1520-0442(1996)009 < 2190:AODT>2.0.CO;2.

Dandonneau, Y., P. Y. Deschamps, J. M. Nicolas, H. Loisel, J. Blanchot, Y. Montel, F. Thieuleux, and G. Bécu (2004), Seasonal and interannual variability of ocean color and composition of phytoplankton communities in the North Atlantic, equatorial Pacific and South Pacific, *Deep Sea Res., Part II*, *51*(1), 303–318, doi:10.1016/j.dsr2.2003.07.018.

Grodsky, S. A., J. A. Carton, S. Nigam, and Y. M. Okumura (2012), Tropical Atlantic biases in CCSM4, *J. Clim.*, *25*(11), 3684–3701.

Hagos, S. M., and K. H. Cook (2009), Development of a coupled regional model and its application to the study of interactions between the West African monsoon and the eastern tropical Atlantic Ocean, *J. Clim.*, *22*(10), 2591–2604, doi:10.1175/2008JCLI2466.1.

Jin, F. F. (1996), Tropical ocean-atmosphere interaction, the Pacific cold tongue, and the El Niño-Southern Oscillation, *Science*, *274*(5284), 76.

Jin, F. F. (1997), An equatorial ocean recharge paradigm for ENSO. Part I: Conceptual model, *J. Atmos. Sci.*, *54*(7), 811–829, doi:10.1175/1520-0469(1997)054 < 0811:AEORPF>2.0.CO;2.

Jin, F. F., J. Boucharel, and I. I. Lin (2014), Eastern Pacific tropical cyclones intensified by El Niño delivery of subsurface ocean heat, *Nature*, *516*(7529), 82–85.

Li, G., and S. P. Xie (2012), Origins of tropical-wide SST biases in CMIP multi-model ensembles, *Geophys. Res. Lett.*, *39*, L22703, doi:10.1029/2012GL053777.

McGregor, S., N. J. Holbrook, and S. B. Power (2007), Interdecadal sea surface temperature variability in the equatorial Pacific Ocean, Part I: The role of off-equatorial wind stresses and oceanic Rossby waves, *J. Clim.*, *20*(11), 2643–2658, doi:10.1175/JCLI4145.1.

Muñoz, E., B. Kirtman, and W. Weijer (2011), Varied representation of the Atlantic meridional overturning across multidecadal ocean reanal-yses, *Deep Sea Res., Part II*, *58*(17), 1848–1857.

Muñoz, E., W. Weijer, S. A. Grodsky, S. C. Bates, and I. Wainer (2012), Mean and variability of the tropical Atlantic Ocean in the CCSM4, *J. Clim.*, *25*(14), 4860–4882.

Nnamchi, H. C., J. Li, F. Kucharski, I. S. Kang, N. S. Keenlyside, P. Chang, and R. Farneti (2015), Thermodynamic controls of the Atlantic Niño, *Nat. Commun.*, *6*, 8895.

Nnamchi, H. C., J. Li, F. Kucharski, I. S. Kang, N. S. Keenlyside, P. Chang, and R. Farneti (2016), An equatorial–extratropical dipole structure of the Atlantic Niño, *J. Clim.*, *29*(20), 7295–7311.

Richter, I., and S. P. Xie (2008), On the origin of equatorial Atlantic biases in coupled general circulation models, *Clim. Dyn.*, *31*(5), 587–598, doi:10.1007/s00382-008-0364-z.

Richter, I., S. P. Xie, S. K. Behera, T. Doi, and Y. Masumoto (2014), Equatorial Atlantic variability and its relation to mean state biases in CMIP5, *Clim. Dyn.*, *42*(1–2), 171–188.

Taylor, K. E., R. J. Stouffer, and G. A. Meehl (2012), An overview of CMIP5 and the experiment design, *Bull. Am. Meteorol. Soc.*, *93*(4), 485–498.

Voldoire, A., M. Claudon, G. Caniaux, H. Giordani, and R. Roehrig (2014), Are atmospheric biases responsible for the tropical Atlantic SST biases in the CNRM-CM5 coupled model?, *Clim. Dyn.*, *43*(11), 2963–2984.

Wang, L. C., F. F. Jin, C. R. Wu, and H. H. Hsu (2017), Dynamics of upwelling annual cycle in the equatorial Atlantic Ocean, *Geophys. Res. Lett.*, *44*, 3737–3743, doi:10.1002/2017GL072588.

Weingartner, T. J., and Weisberg R. H. (1991), On the annual cycle of equatorial upwelling in the Central Atlantic Ocean, *J. Phys. Oceanogr.*, *21*, 68–82, doi:10.1175/1520-0485(1991)021 < 0068:OTACOE>2.0.CO;2.

Wolff, J., E. Maier-Reimer, and S. Legutke (1997), The Hamburg Ocean Primitive Equation model, *Tech. Rep. 13*, 98 pp., Dtsch. Klimarechen-zentrum, Hamburg, Germany.

Zebiak, S. E., and M. A. Cane (1987), A model El Niño–Southern Oscillation, *Mon. Weather Rev.*, *115*(10), 2262–2278, doi:10.1175/1520-0493(1987)115 < 2262:AMENO>2.0.CO;2.

Zhai, F., and D. Hu (2013), Revisit the interannual variability of the North Equatorial Current transport with ECMWF ORA-S3, *J. Geophys. Res. Oceans*, *118*, 1349–1366, doi:10.1002/jgrc.20093.